Oscillating Cascade Aerodynamics by an Experimental Influence Coefficient Technique

Daniel H. Buffum*
NASA Lewis Research Center, Cleveland, Ohio 44135
and
Sanford Fleeter†
Purdue University, West Lafayette, Indiana 47907

Fundamental experiments are performed in the NASA Lewis Transonic Oscillating Cascade Facility to investigate the torsion-mode, unsteady aerodynamics of a biconvex airfoil cascade at realistic values of the reduced frequency for all interblade phase angles at a specified mean-flow condition. In particular, an unsteady aerodynamic influence coefficient technique in which only one airfoil in the cascade is oscillated at a time and the resulting airfoil surface unsteady pressure distribution measured on one dynamically instrumented airfoil is developed and utilized. The unsteady aerodynamics of an equivalent cascade with all of the airfoils oscillating at a specified interblade phase angle are then determined through a vector summation of these data. The cascade aerodynamics, as computed from these influence coefficients, are correlated with data obtained in this cascade with all airfoils oscillating at several interblade phase angle values. The influence coefficients are then utilized to determine the unsteady aerodynamics of the cascade for all interblade phase angles with these data subsequently correlated with predictions from a linearized unsteady cascade model.

Nomenclature

C = airfoil chord
C_m = unsteady moment coefficient about midchord
$\hat{C}_m^n$ = unsteady aerodynamic moment influence coefficient for n^{th} airfoil
C_p = unsteady pressure coefficient $p_1/\frac{1}{2}\rho V^2\alpha_1$
$\bar{C}_p$ = steady static pressure coefficient, $(\bar{p}_{in} - \bar{p})/\frac{1}{2}\rho V^2$
$\hat{C}_p^n$ = unsteady pressure influence coefficient for n^{th} airfoil
k = reduced frequency $\omega C/2V$
M = inlet Mach number
$\bar{p}$ = airfoil surface static pressure
p_1 = first harmonic of airfoil surface unsteady static pressure
$\bar{p}_{in}$ = inlet steady static pressure
S = airfoil spacing
V = inlet velocity
x = chordwise coordinate
y = coordinate normal to chordwise direction
α_0 = mean flow incidence angle
α_1 = torsional oscillation amplitude
γ = stagger angle
ΔC_p = unsteady pressure difference coefficient
β = interblade phase angle (positive when airfoil n leads airfoil n-1)
ρ = inlet density
τ = maximum airfoil thickness
ω = airfoil oscillatory frequency

Presented as Paper 88-2815 at the AIAA/ASME/SAE/ASEE 24th Joint Propulsion Conference, Boston, MA, July 11-13, 1988; received Aug. 22, 1988; revision received July 24, 1989.

*Aerospace Engineer.
†Professor, School of Mechanical Engineering, Thermal Sciences and Propulsion Center.

Introduction

IN the rotating blade rows of turbomachines and propellers, the possibility of flutter is a continual concern. Unfortunately, the ability to predict flutter has not kept pace with the overall advances and new requirements of turbomachine and turboprop designs. Consequently, the development of analyses to predict oscillating cascade aerodynamics is of fundamental research interest. To direct the development of these advanced unsteady aerodynamic models and to evaluate these as well as existing analyses, data from oscillating cascade experiments are needed. However, due to the complexity of these experiments, few results are available at realistic reduced frequency values, particularly in the high subsonic and transonic flow regimes.

Oscillating cascade experiments are complex and time consuming because the unsteady aerodynamics of the cascade must be measured, not only for every new steady-flow condition and reduced frequency but also for each interblade phase angle value. In principle, however, oscillating cascade data can be obtained for all interblade phase angles at a specified mean flow condition and reduced frequency through simpler experiments. In particular, an unsteady aerodynamic influence coefficient technique can be utilized when the unsteady disturbances are small, such as in the flutter stability problem. In this technique, only one airfoil in the cascade is oscillated with the resulting airfoil surface unsteady pressure distributions measured on the oscillating airfoil and its stationary neighbors. The unsteady aerodynamics of an equivalent cascade with all airfoils oscillating at a specified interblade phase angle are then determined through a vector summation of these influence coefficient data.

To use this unsteady aerodynamic influence coefficient technique to acquire unsteady aerodynamic data that the designer and analyst will use, it is first necessary to experimentally verify the validity of this technique. This requires the correlation of oscillating cascade data determined from the unsteady aerodynamic influence coefficients with corresponding data for a cascade in which all airfoils oscillate at specific interblade phase angles. Several investigations have been di-

rected at this experimental verification. However, the results are inconclusive. Hanamura[1] had good results using the influence coefficient technique, but their experiment, performed in a water channel, was limited to incompressible flow. Davies and Whitehead[2] performed such experiments in an annular cascade at high subsonic inlet conditions and reduced frequencies up to 0.1. Unfortunately, the validity of the unsteady aerodynamic influence technique cannot be assessed due to the data scatter. The effect of oscillating a single airfoil and three airfoils in a cascade at low speed was studied by Tanaka.[3] Although a summation of the influence coefficients was not presented, the technique appears promising for data in regions of attached flow. In supersonic inlet Mach number experiments at the Office National d'Etudes et de Recherches Aéronautique (ONERA),[4] the summation of influence coefficients has been compared to data for a linear cascade with two airfoils oscillating. The limited scope of these experiments precludes conclusions concerning the validity of the influence coefficient technique.

In this paper, the NASA Lewis Transonic Oscillating Cascade Facility is utilized to investigate the torsion-mode, unsteady aerodynamics of a biconvex airfoil cascade at realistic values of the reduced frequency for all interblade phase angles at a specified mean-flow condition. This is accomplished by 1) experimentally verifying the unsteady aerodynamic influence coefficient technique and 2) subsequently utilizing this experimental technique to determine the unsteady aerodynamics of an oscillating cascade for all interblade phase angles. In particular, in a subsonic compressible flow at realistic reduced frequencies, unsteady aerodynamic influence coefficient data are obtained by oscillating one airfoil in the cascade and measuring the resulting airfoil surface unsteady pressure distributions on the oscillating airfoil and its stationary neighbors. These data are correlated with corresponding oscillating cascade data, i.e., data obtained in this cascade with all airfoils oscillating at several interblade phase angle values. The unsteady aerodynamic influence coefficients are then utilized to determine the unsteady aerodynamics of the cascade for all interblade phase angles with these data subsequently correlated with predictions from a linearized unsteady cascade model.

Theory

Figure 1 schematically depicts the two-dimensional finite cascade representation of a rotor blade row. For a given mean flowfield and reduced frequency of oscillation, the cascade unsteady aerodynamics can be written in terms of linearly combined influence coefficients, which can be determined both experimentally and analytically.

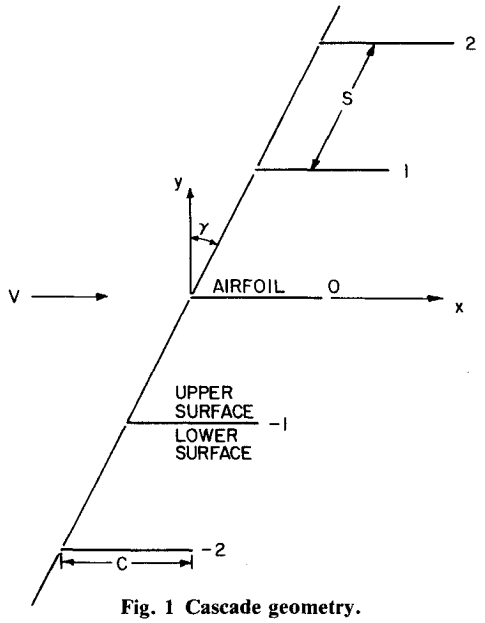

Fig. 1 Cascade geometry.

For a finite airfoil cascade with 2N + 1 airfoils executing constant amplitude harmonic oscillations with a constant interblade phase angle β the unsteady aerodynamic moment C_m acting on the reference airfoil, taken as airfoil 0 for convenience, can be expressed as a Fourier series of the influence coefficients $\hat{C}_m^n$ [see Eq. (1)]. These influence coefficients can be experimentally measured in a finite cascade by oscillating a single airfoil and measuring the unsteady aerodynamics on the oscillating airfoil and its stationary neighbors.

$$C_m(\beta) = \sum_{n=-N}^{N} \hat{C}_m^n e^{in\beta} \tag{1}$$

where $\hat{C}_m^n$ is the complex unsteady aerodynamic moment influence coefficients, which define the unsteady moment developed on the reference airfoil due to the motion of airfoil n with all of the other airfoils in the cascade stationary.

Mathematical models for an infinite cascade of airfoils oscillating with a specified interblade phase angle can also be used to determine these unsteady aerodynamic influence coefficients. For this case, the number of airfoils is taken as infinite with the influence coefficients subsequently determined by the inversion of Eq. (1).

$$\hat{C}_m^n = \frac{1}{2\pi}\int_{-\pi}^{\pi} C_m(\beta) e^{-in\beta}\, d\beta \tag{2}$$

Analytically determined unsteady aerodynamic influence coefficients can thus be determined from oscillating cascade mathematical models by integrating over the complete interblade phase angle interval, Eq. (2). Using these influence coefficients in Eq. (1) then enables analytical results for a finite number of airfoils oscillating in an infinite cascade to be determined.

Oscillating Cascade Facility

The NASA Lewis Transonic Oscillating Cascade Facility depicted in Fig. 2 is a linear cascade wind tunnel capable of test section Mach numbers approaching unity. Air drawn from the atmosphere passes through a smoothly contracting inlet section into a constant area 9.78 × 19.21-cm test section and then through a diffuser and exhaust header which has a nominal pressure of 3.0 N/cm^2. The flow rate is controlled by two valves located in the header. Upstream of the test section, a partitioned bleed system removes the boundary layers on each end wall. The boundary layers on the upper and lower cascade walls are removed through tailboard slots.

A major feature of this facility is the high speed mechanical drive system, which imparts controlled torsional oscillations to any or all of the nine cascaded airfoils. Nine barrel cams, each with a six-cycle sinusoidal groove machined into its periphery, are mounted on a common shaft driven by a 74.6-kW electric motor. Connecting arms, joined to one end of each airfoil by trunnions, have buttons on the opposite end to follow the cam grooves. The amplitude of the airfoil motion is ± 1.2 deg dictated by the cam and follower geometry. With all of the airfoils oscillating, different interblade phase angle

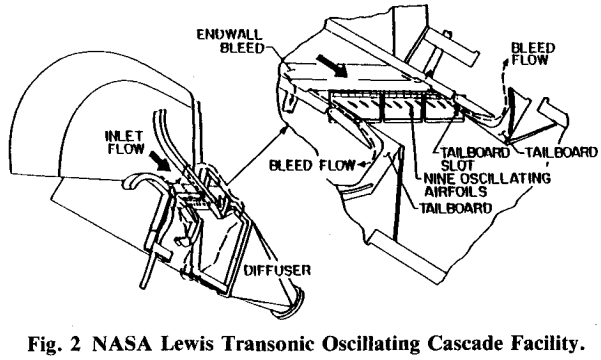

Fig. 2 NASA Lewis Transonic Oscillating Cascade Facility.

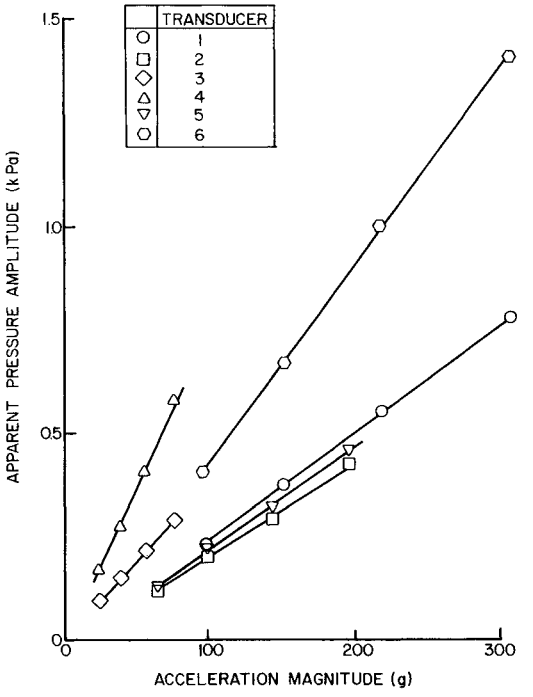

Fig. 3 Dynamic pressure transducer acceleration response.

oscillations are achieved by changing the relative positions of the cams. In this investigation, the maximum oscillatory frequency is 350 Hz, corresponding to a reduced frequency of 0.390 with a cascade inlet Mach number of 0.65.

Airfoils and Instrumentation

The cascade is made of nine uncambered biconvex airfoils with a chord of 7.62 cm, a thickness-to-chord ratio of 0.076, a solidity of 1.3, and a 53-deg stagger angle. The radius of curvature of the airfoil surfaces is 27.4 cm with the leading and trailing edges rounded with a 0.025-cm radius of curvature. The airfoils are supported by two midchord trunnions resulting in a midchord elastic axis location.

The primary data are the complex unsteady surface pressures on the oscillating cascaded airfoils. These data are obtained by six Kulite transducers flush-mounted symmetrically along the chord on one airfoil surface, Table 1, and then statically calibrated. Thus, to obtain the unsteady pressure data for both surfaces during simultaneous oscillation of the airfoils, the experiments are performed in two phases with data acquired on one surface at a time. The transducers, each with an active sensor diameter of 0.097 cm, 1.3% of the airfoil chord, are placed in milled slots and potted in RTV to isolate them from airfoil strain. For the influence coefficient experiments, a thin coating of RTV protects the sensor surface and fairs it into the contour of the airfoil.

During oscillation, the pressure transducers are subject to accelerations which may produce significant apparent pressure signals. To quantify this effect, the instrumented airfoil was oscillated at several frequencies under no-flow or zero-mean velocity conditions. Figure 3 shows the amplitude response of the six coated transducers as a function of the acceleration magnitude. The response is a linear function of the acceleration, implying that the acoustic response, which is expected to vary with the airfoil velocity magnitude, is dominated by the acceleration response. Significant amplitude variation is apparent among the transducers and is probably due to installation effects. The phase angle variation with frequency was linear and small for all the transducers.

The time-variant position of the reference oscillating airfoil is determined by a capacitance-type proximity sensor, which produces a voltage proportional to the air gap between it and an adjacent object. This sensor is positioned to face a six-cycle sinusoidally shaped cam mounted on the same shaft as the airfoil drive cams and to be in phase with the reference airfoil motion. As shown in the sample in Fig. 4, this signal is virtually noise free.

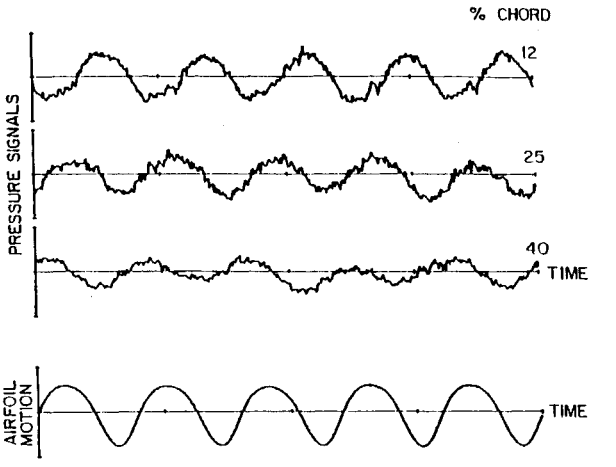

Fig. 4 Time variant signals.

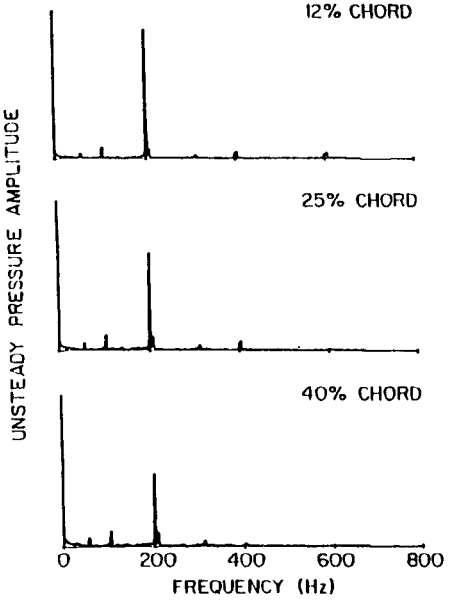

Fig. 5 Averaged pressure spectra.

Table 1 Airfoil and cascade geometry

Airfoil	
Type	biconvex, no camber
Surface radius of curvature	27.4 cm
Leading and trailing edge radii of curvature	0.025 cm
Maximum airfoil thickness, τ	0.58 cm
Chord, C	7.62 cm
Elastic axis	midchord
Dynamic pressure transducer locations, (% chord)	12, 25, 40 60, 75, 88
Cascade	
Number of airfoils	9
Solidity, C/S	1.3
Spacing, S	5.86 cm
Stagger angle, τ	53 deg
Amplitude of motion	1.2 deg

Data Acquisition and Analysis

All of the unsteady signals are ac coupled and recorded on magnetic tape for postexperiment processing. During tape

playback, the signals are simultaneously digitized at rates sufficient to capture at least three harmonics of the oscillation frequency with 32,768 samples taken per channel. Each data channel is divided into blocks, typically with 2048 samples, and then Fourier decomposed and referenced to the airfoil motion by subtracting the phase of the motion signal from the pressure signal. With all of the transducer signal blocks decomposed, the results are averaged and in the case of the influence coefficient data, the acceleration responses are subtracted vectorally. To minimize errors due to spectral leakage, an interpolation scheme is applied to the decomposed results in conjuction with a Hanning window.[5]

To demonstrate this data analysis technique, the pressure transducer signals shown in Fig. 4 are considered. The resulting averaged pressure spectra (Fig. 5) are characterized by a large spike at the oscillation frequency, in this case 200 Hz, some small spikes at higher harmonics of the oscillation frequency, and other small spikes caused by wind tunnel tones.

The final unsteady pressure data are defined by the complex dynamic pressure and pressure difference coefficients, C_p and ΔC_p, Eq. (3). These complex data are presented in the format of a magnitude and phase referenced to the airfoil motion with a positive phase corresponding to the unsteady pressure leading the airfoil motion

$$C_p(x) = \frac{p_1(x)}{\frac{1}{2}\rho V^2 \alpha_1} \qquad \Delta C_p = C_{pl} - C_{pu} \tag{3}$$

where p_1 is the first harmonic of the unsteady static pressure, ρ and V are the inlet values of density and velocity, and α_1 is the torsional oscillation amplitude.

The summation of dynamic pressure coefficient influences is analogous to the moment coefficient summation of Eq. (1). With $\hat{C}_p^n$ being the complex pressure influence coefficient, the dynamic pressure coefficient is calculated using Eq. (4)

$$C_p(\beta) = \sum_{n=-N}^{N} \hat{C}_p^n e^{in\beta} \tag{4}$$

Torsion mode unsteady moment coefficients, C_m, are calculated from the unsteady pressure difference data, Eq. (5). This is accomplished by 1) assuming there is a zero pressure difference at the leading and trailing edges of the airfoil; 2) fitting a smooth curve through the chordwise distribution of the data; and 3) numerically integrating the resulting chordwise distribution of the pressure difference.

$$C_m = \int_0^1 \left(\frac{1}{2} - \frac{x}{C}\right) \Delta C_p d\left(\frac{x}{C}\right) \tag{5}$$

Results

The steady-state cascade aerodynamics and the unsteady aerodynamic influence coefficient technique are experimentally investigated at steady-flow conditions defined by an incidence angle of 0 deg and an inlet Mach number of 0.65 resulting in an entirely subsonic flowfield.

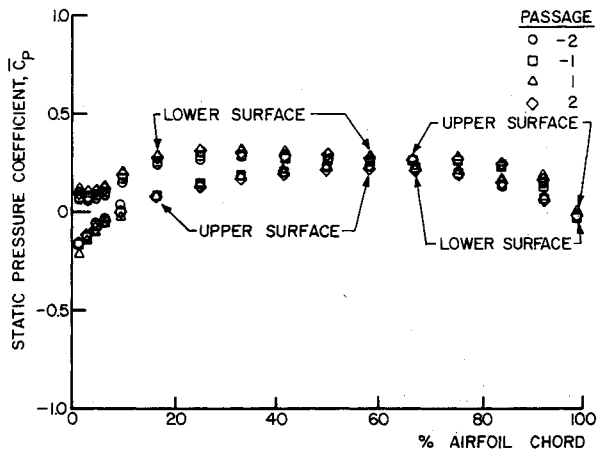

Fig. 6 Steady-flow, airfoil surface pressure distributions.

Steady-State Aerodynamics

The cascade airfoil surface steady-state aerodynamics are defined in Fig. 6. Also presented is a demonstration of the steady-state cascade periodicity with airfoil surface pressure distributions presented for the four cascade passages surrounding the center airfoil. The passage 1 data are the pressure distributions for the upper surface of airfoil 0 (the center airfoil) and the lower surface of airfoil 1. Passage -1 data are for the lower surface of airfoil 0 and the upper surface of airfoil -1, etc. The good periodicity of the cascade flowfield is apparent. Also, the airfoils are loaded due to cascading effects even though the upstream flow direction was chosen to obtain zero incidence. The cascade exit Mach number is 0.65, and the zero pressure difference condition at the trailing edge is satisfied.

Unsteady Aerodynamics

With the instrumented (reference) airfoil in position 0 as defined in Fig. 1, unsteady data are acquired on this airfoil with the airfoils in positions -2, -1, 0, $+1$, and $+2$ individually oscillating at reduced frequencies of 0.223 and 0.390. First, the unsteady pressure influence coefficients on the individual surfaces of the reference instrumented airfoil are considered. These data are then correlated with 1) predictions from the unsteady, small perturbation, subsonic flat plate cascade analyses of Refs. 6 and 7; and 2) baseline data obtained in experiments where all of the airfoils in the cascade are oscillating at the same time for interblade phase angles of 0, 90 and -90 deg. In these experiments, the airfoil motion is defined by the change in the incidence angle with time

$$\alpha(t) = \alpha_1 Re\{e^{(i\omega t)}\} \tag{6}$$

α_1 is the oscillatory amplitude of 1.2 deg.

Unsteady Airfoil Surface Influence Coefficients

Figures 7-11 present the chordwise distribution of the dynamic pressure influence coefficients on the individual sur-

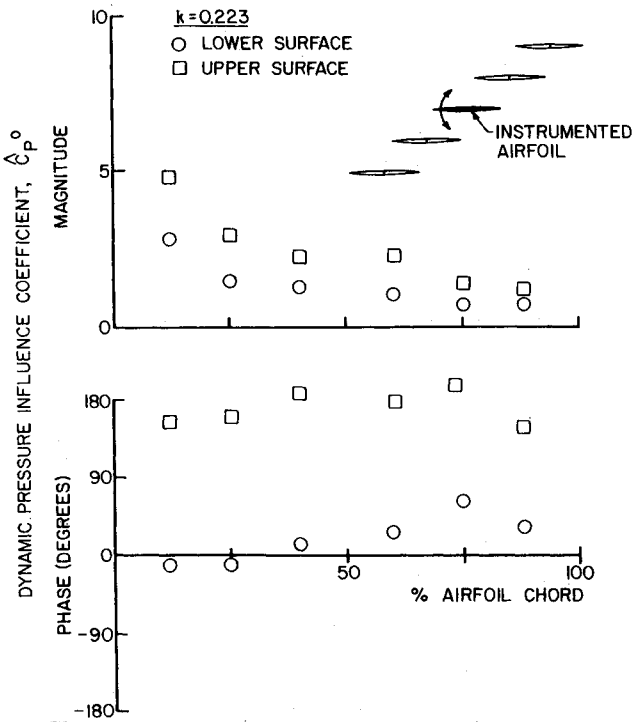

Fig. 7 Dynamic pressure influence coefficient, airfoil 0 oscillating.

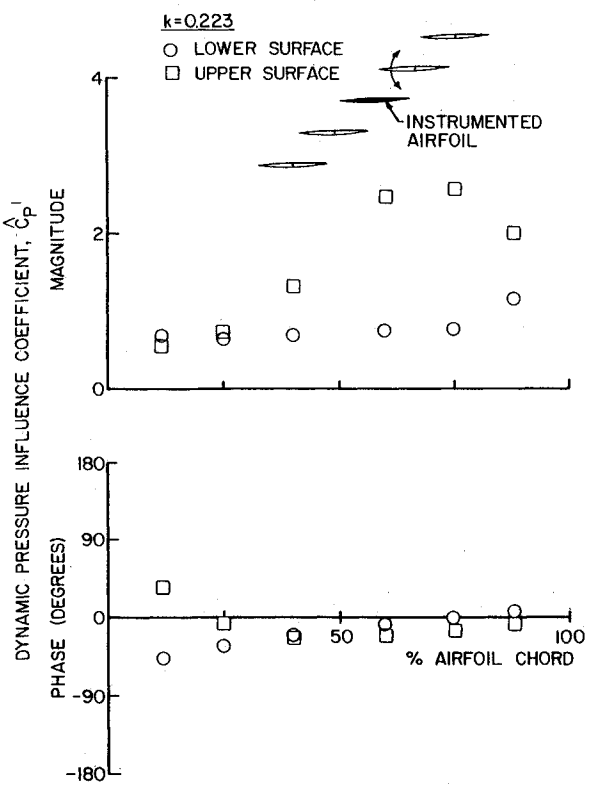

Fig. 8 Dynamic pressure influence coefficient, airfoil 1 oscillating.

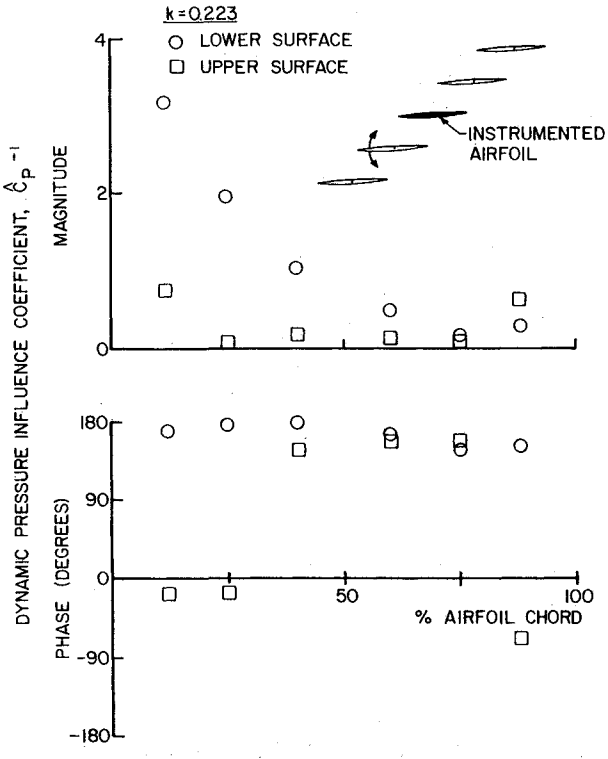

Fig. 9 Dynamic pressure influence coefficient, airfoil, −1 oscillating.

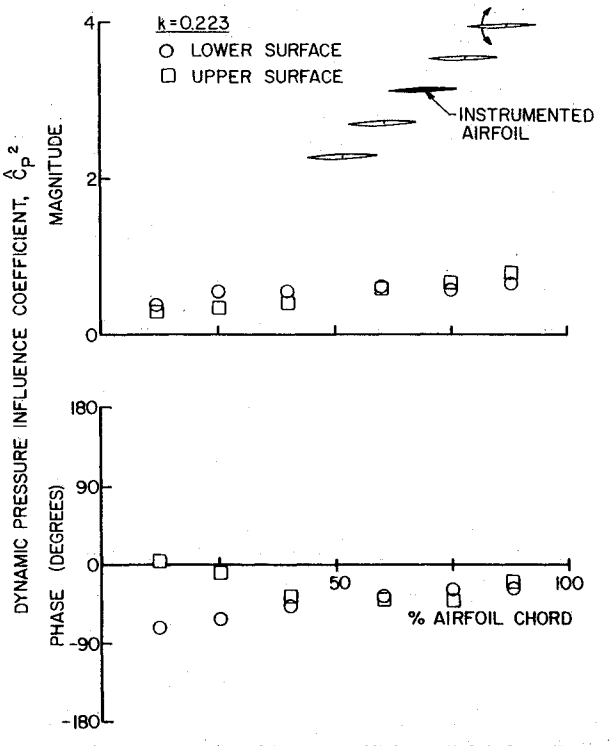

Fig. 10 Dynamic pressure influence coefficient, airfoil 2 oscillating.

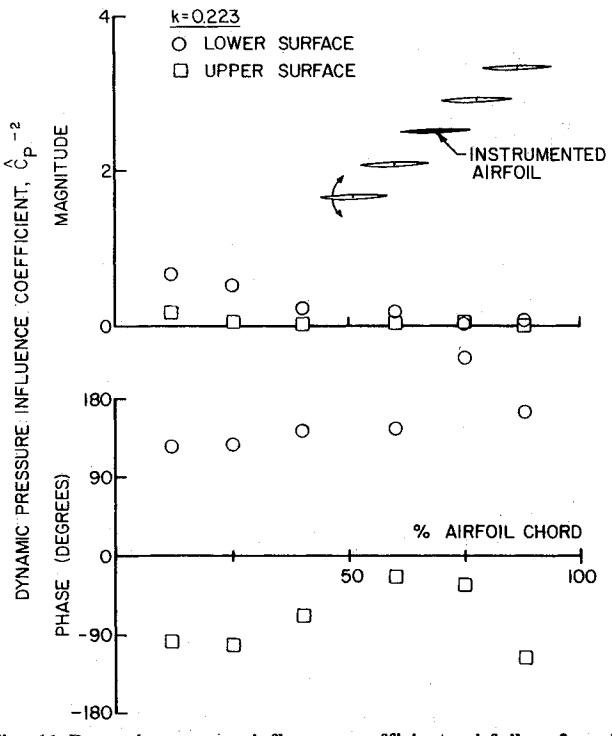

Fig. 11 Dynamic pressure influence coefficient, airfoil −2 oscillating.

faces of the position 0 reference airfoil with the oscillating airfoil in the five relative positions defined by −2 through +2.

The self-induced oscillating airfoil unsteady pressure response is shown in Fig. 7. Namely, this figure presents the unsteady pressures on the surfaces of the reference airfoil with the reference airfoil itself oscillating. The magnitude of the unsteady pressure on each surface attains a maximum at the leading edge, tending towards zero at the trailing edge, with the magnitude generally larger on the upper surface. Also, the upper surface phase data are out of phase with the airfoil motion.

Figures 8 and 9 show the unsteady pressure effect on the surfaces of the stationary instrumented reference airfoil due to individually oscillating its nearest neighbors, i.e., individually oscillating the airfoils in positions +1 and −1, respectively. As seen, oscillating the neighboring airfoil has a relatively large effect on the magnitude of the unsteady pressure on the reference airfoil surface nearest to the oscillating airfoil. In particular, Fig. 8 shows that oscillating the airfoil located

immediately above the reference airfoil results in relatively large unsteady pressure fluctuations over the aft half of the reference airfoil upper surface with the lower surface pressure coefficient magnitude nearly constant and a nearly linear variation in the lower surface phase angle. With the oscillating airfoil positioned immediately beneath the reference airfoil, Fig. 9 shows that there are relatively large pressure fluctuations over the leading quarter of the reference airfoil lower surface, whereas the upper surface has only a small response in the leading and trailing edge regions with the lower surface oscillations out of phase with the motion.

The effect on the unsteady pressure on the surfaces of the instrumented reference airfoil due to oscillating the airfoils which are in the +2 and −2 positions are shown in Figs. 10 and 11, respectively. As expected for this case with the oscillating airfoils further distanced from the reference airfoil, the magnitude of the unsteady pressures on the reference airfoil are reduced compared to the previous results where the nearest neighbors were oscillated. Also, with the oscillating airfoil

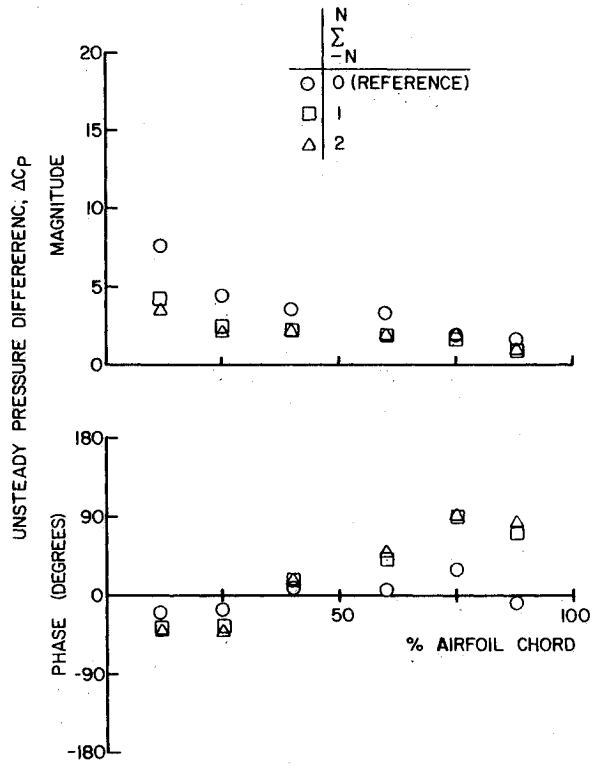

Fig. 12 Unsteady pressure difference on reference airfoil, $\beta = 0$ deg, $k = 0.223$.

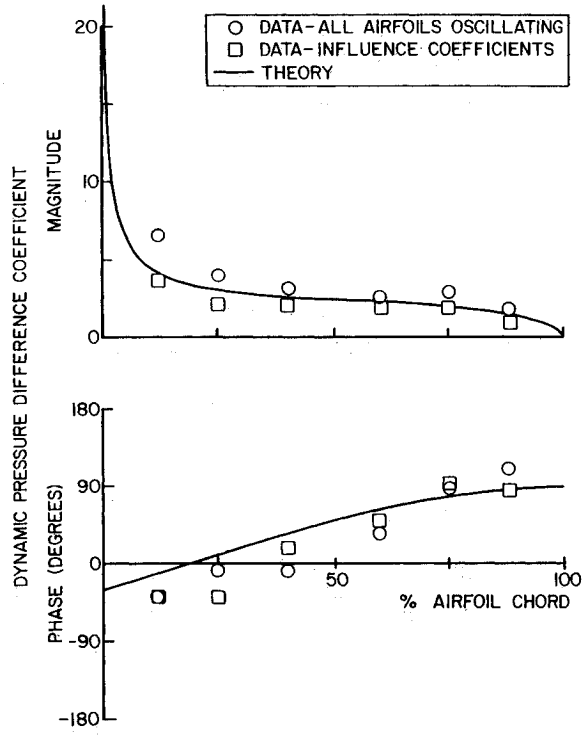

Fig. 14 Dynamic pressure difference coefficient distribution, $\beta = 0$ deg, $k = 0.223$.

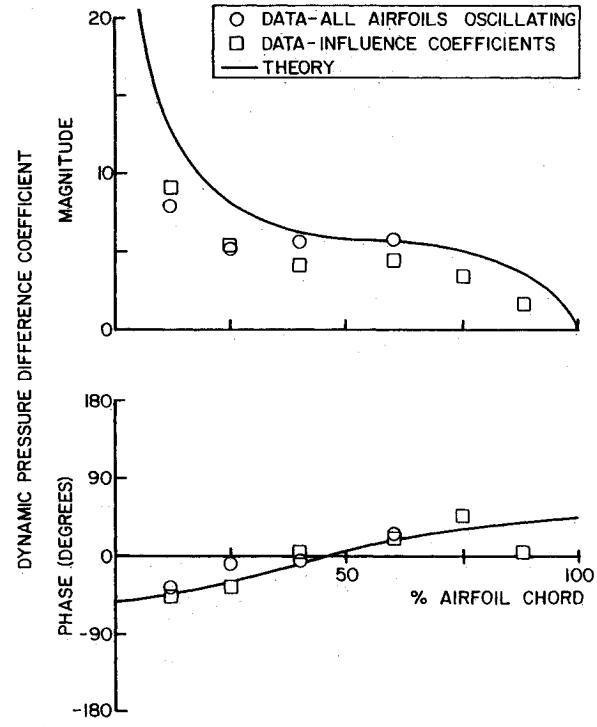

Fig. 13 Dynamic pressure difference coefficient distribution, $\beta = -90$ deg, $k = 0.223$.

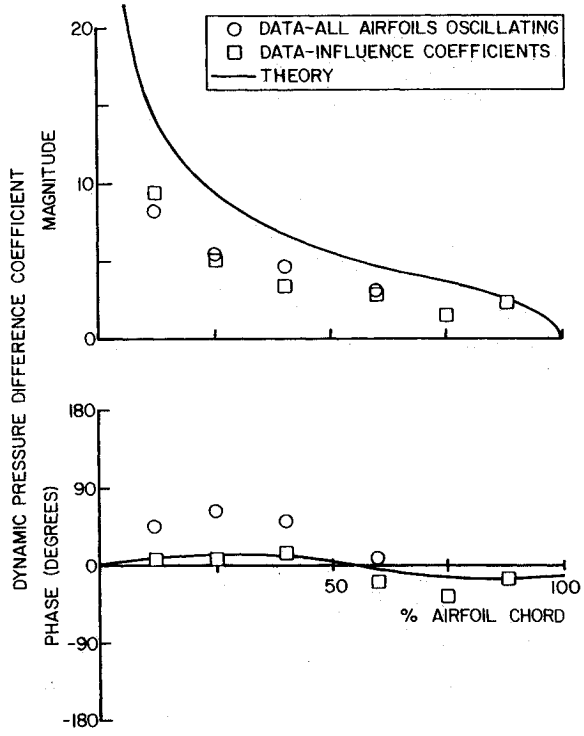

Fig. 15 Dynamic pressure difference coefficient distribution, $\beta = 90$ deg, $k = 0.223$.

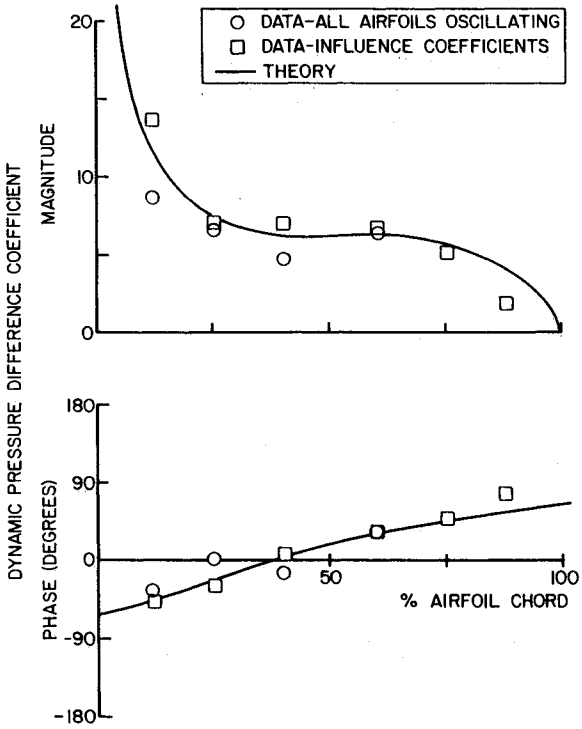

Fig. 16 Dynamic pressure difference coefficient distribution, $\beta = -90$ deg, $k = 0.390$.

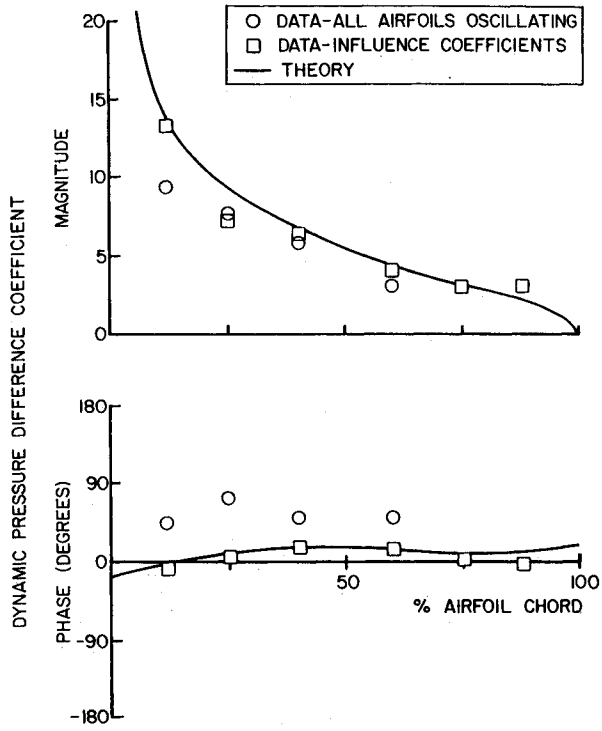

Fig. 18 Dynamic pressure difference coefficient distribution, $\beta = 90$ deg, $k = 0.390$.

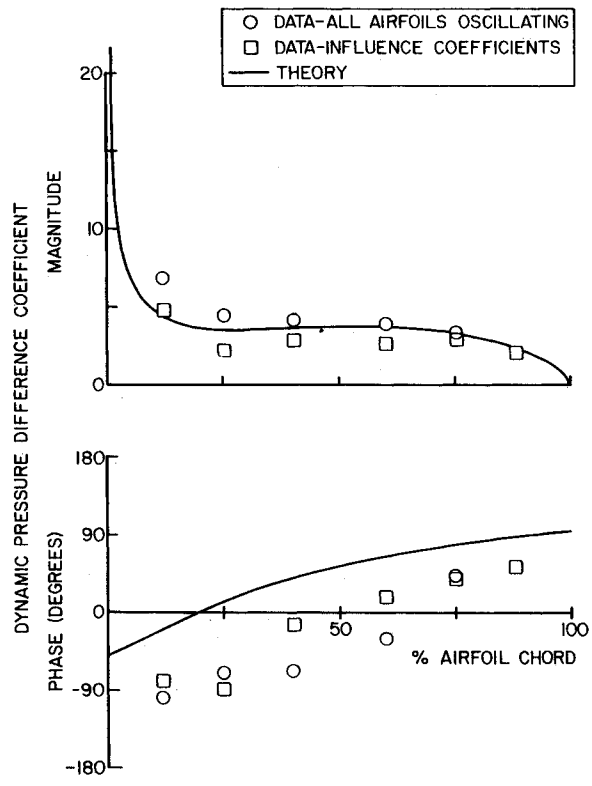

Fig. 17 Dynamic pressure difference coefficient distribution, $\beta = 0$ deg, $k = 0.390$.

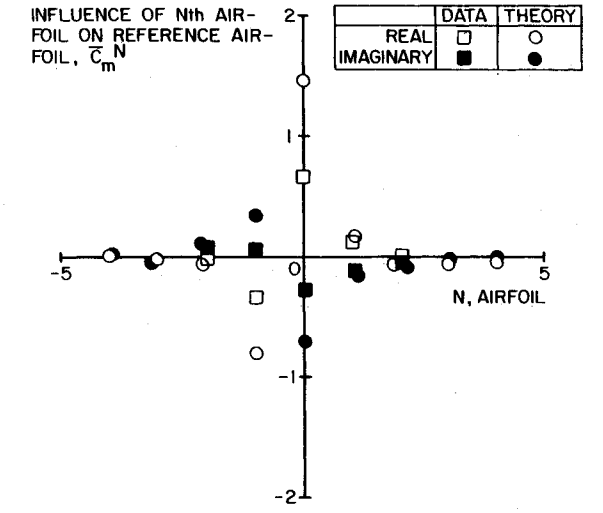

Fig. 19 Influence of N^{th} airfoil on reference airfoil unsteady aerodynamic moment, $k = 0.223$.

above the reference airfoil in position +2, the amplitudes are nearly the same for the two surfaces, but there is an unsteady load on the airfoil due to the phase difference at the two forward transducers, Fig. 10. For the oscillating airfoil in position −2, Fig. 11 shows that the lower surface response is negligible, whereas the upper surface has a small response over the forward two-thirds of the airfoil.

Unsteady Pressure Differences

The summation of the oscillating airfoil surface unsteady pressure influence coefficients and the determination of the unsteady pressure difference coefficient is shown in Fig. 12. In particular, the 0.223-reduced frequency data are presented as a dynamic pressure difference coefficient for an interblade phase angle of 0 deg with N specifying the limits of the sum per Eq. 4. Thus $N = 0$ corresponds to the self-induced unsteady aerodynamic response. The influence coefficient series is rapidly convergent with only the reference airfoil and its two immediate neighbors having a significant effect on the resulting dynamic pressure difference distribution.

The influence coefficient determined chordwise distribution of the unsteady airfoil surface pressure difference data are correlated with corresponding data obtained in experiments in which all of the airfoils in the cascade are oscillating at the same time with a constant interblade phase angle value and

also with the flat-plate cascade predictions in Figs. 13–15 at a 0.223-reduced frequency value and in Figs. 16–18 for a reduced frequency of 0.390. Due to the failure of several dynamic pressure transducers, some data points for all airfoils oscillating are omitted.

The complex unsteady aerodynamic influence coefficient data generally exhibit good correlation with both the oscillating cascade data and the linearized theory. In particular, the influence coefficient magnitude data generally exhibit good correlation with both the oscillating cascade data and the prediction. An exception to this is the lower reduced frequency +90 deg interblade phase angle data (Fig. 15) where the experimental data are in good agreement with each other but the theoretical magnitude is significantly greater than the data.

The two sets of unsteady pressure difference phase data are in good agreement with one another and with the prediction at an interblade phase angle of −90 deg, Figs. 13 and 16. For in-phase motions, Figs. 14 and 17 show that the two sets of phase data are decreased relative to the prediction, particularly at the higher reduced frequency, with the influence coefficient data centered between the prediction and the oscillating cascade data at 40% and 60% of chord. At an interblade phase angle of +90 deg (Figs. 15 and 18), the influence coefficient phase data are in good agreement with the prediction with the oscillating cascade data increased in value.

Unsteady Aerodynamic Moment

Figures 19 and 20 show the complex unsteady aerodynamic moment influence coefficients calculated from the experimental data using Eq. (5) and the predictions for reduced frequencies of 0.223 and 0.390, respectively, in the format of the influence of the Nth airfoil in the cascade on the 0th (reference) airfoil. The unsteady aerodynamic moment on the reference airfoil is seen to be a strong function of the unsteady aerodynamics associated with oscillating the reference airfoil itself and the two adjacent airfoils. The experimentally determined influence of airfoils −1 and 0 are significantly less than predicted, particularly at $k = 0.223$.

The resulting measured and predicted imaginary part of the unsteady aerodynamic moment on the reference airfoil of an infinite cascade for all interblade phase angles for reduced frequencies of 0.223 and 0.390 are presented in Figs. 21 and 22, respectively. It should be noted that the influence coefficient data are valid for all interblade phase angles.

In general, there is trendwise agreement between the influence coefficient data and the interblade phase-angle oscillating cascade data with the lower reduced frequency exhibiting better correlation. For $k = 0.39$ and $\beta = +90$ deg, the oscillating cascade data indicate stability; whereas the influence coefficient data indicate marginal stability. There is also trendwise agreement between the influence coefficient data and the infinite oscillating cascade predictions; although for $\beta = -90$ deg, the predictions have significantly smaller values.

Figures 21 and 22 also present the theoretical results for the case of a finite number of oscillating airfoils in the cascade. For the subresonant interblade phase angles, the finite and infinite oscillating airfoil cascade predictions are in good agreement with one another. However, in the vicinity of the acoustic resonance points, the predictions are not in good agreement. In particular, to capture the rapidly changing unsteady aerodynamic response in these regions, many more oscillating airfoils in the finite cascade are required. Thus, acoustic resonances will not occur in linear cascade experiments due to the limited number of airfoils in the cascade.

Summary and Conclusions

A series of fundamental experiments have been performed in the NASA Lewis Transonic Oscillating Cascade Facility to

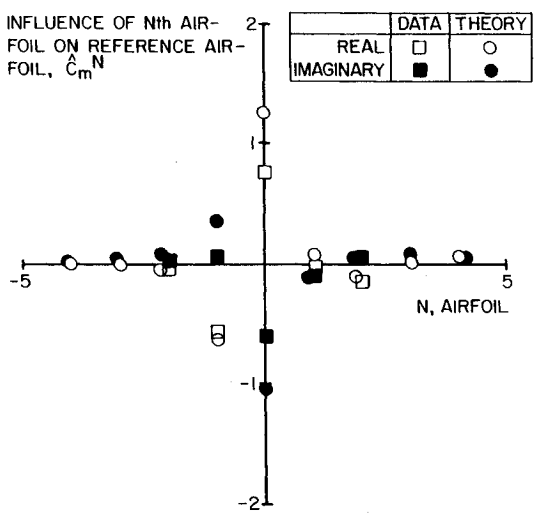

Fig. 20 Influence of N^{th} airfoil on reference airfoil unsteady aerodynamic moment, $k = 0.390$.

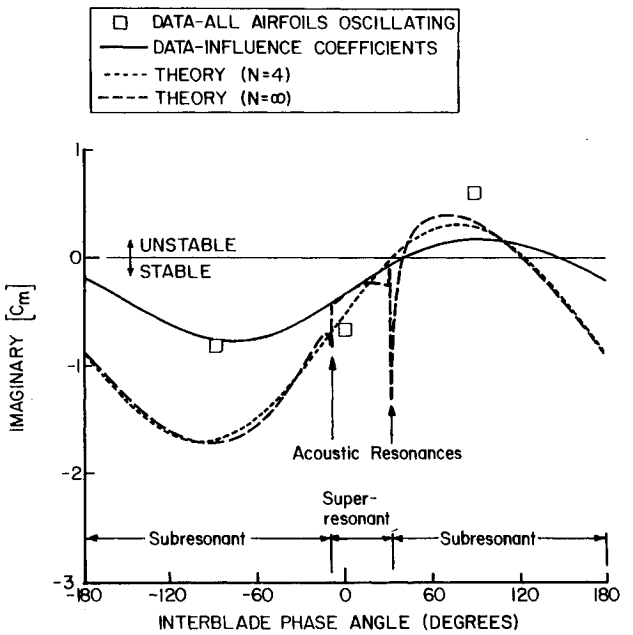

Fig. 21 Imaginary unsteady aerodynamic moment correlation, $k = 0.223$.

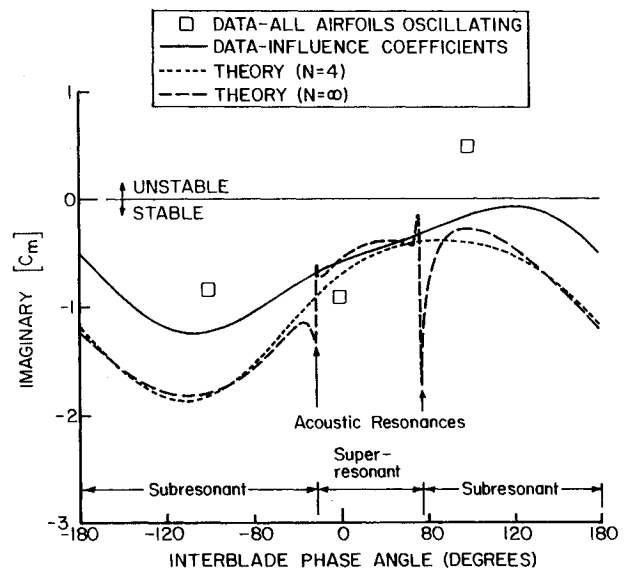

Fig. 22 Imaginary unsteady aerodynamic moment correlation, $k = 0.390$.

investigate the torsion-mode oscillating aerodynamics of a biconvex airfoil cascade. In particular, all interblade phase angles were considered at two realistic high values of the reduced frequency at specific subsonic zero incidence mean-flow conditions. This was accomplished by developing and utilizing an unsteady aerodynamic influence coefficient technique in which only one airfoil in the cascade is oscillated and the resulting airfoil surface unsteady pressures measured on the oscillating airfoil and its stationary neighbors. Vector summation of these data allows determination of the unsteady aerodynamics for arbitrary interblade phase angles of an equivalent cascade with all airfoils oscillating.

Analysis of these data and correlation with both the prediction from the unsteady, small perturbation, subsonic flat-plate cascade analyses and the baseline data obtained in experiments where all of the airfoils in the cascade are oscillating at the same time for interblade phase angles of 0, 90, and -90 deg revealed the following.

1) The unsteady aerodynamic influence coefficient series is rapidly convergent with only the reference airfoil and its two immediate neighbors having a significant effect on the resulting unsteady pressure difference and aerodynamic moment coefficients.

2) With regard to the imaginary part of the unsteady aerodynamic moment, there is trendwise agreement between the influence coefficient data, the oscillating cascade data, and the prediction.

3) The finite and infinite cascade oscillating airfoil predictions are in very good agreement for subresonant interblade phase angles. However, in the vicinity of the acoustic resonance points, the two predictions are not in good agreement with many more oscillating airfoils in the finite cascade required. Thus, acoustic resonances will not occur in linear cascade experiments due to the limited number of airfoils.

In summary, this unsteady aerodynamic influence coefficient experimental technique enables valid subsonic oscillating cascade data to be obtained at realistic values of the reduced frequency for all interblade phase angles.

Acknowledgments

The authors are grateful for the extra efforts of the NASA Lewis Test Installations Division and the Aeropropulsion Facilities Division and for the support and encouragement of Larry Bober and John Groeneweg, which allowed timely completion of this investigation.

References

[1]Hanamura, Y., Tanka, H., and Yamaguchi, K., "A Simplified Method to Measure Unsteady Forces Acting on the Vibrating Blades in Cascade," *Bulletin of the JSME*, Vol. 23, No. 180, June 1980, pp. 880–887.

[2]Davies, M.R.D., and Whitehead, D.S., "Unsteady Aerodynamic Measurements in a Transonic Annular Cascade," *Unsteady Aerodynamics of Turbomachines and Propellers*, Cambridge Univ. Engineering, Cambridge, England, UK, Sept. 1984, pp. 487–502.

[3]Tanaka, H., Yamamoto, K., and Fujimoto, I., "Unsteady Aerodynamic Response of Cascade Blades in Pitching Oscillation with Flow Separation," *Unsteady Aerodynamics of Turbomachines and Propellers*, Cambridge Univ. Engineering, Cambridge, England, UK Sept. 1984, pp. 397–410.

[4]Szechenyi, E., "Fan Blade Flutter-Single Blade Instability or Blade to Blade Coupling?" American Society of Mechanical Engineers, New York, *ASME Paper 85-GT-216*, March 1985.

[5]Burgess, J.C., "On Digital Spectrum Analysis of Periodic Signals," *Journal of the Acoustical Society of America*, Vol. 58, No. 3, Sept. 1975, pp. 556–567.

[6]Smith, S.N. "Discrete Frequency Sound Generation in Axial Flow Turbomachines," Cambridge Univ. Rept., Cambridge, England, UK, *CUED/A-Turbo/TR29*, 1971.

[7]Fleeter, S., "Fluctuating Lift and Moment Coefficients for Cascaded Airfoils in a Nonuniform Compressible Flow," *Journal of Aircraft*, Vol. 10, No. 2, Feb. 1973, pp. 93–98.